Journal of Statistical Physics (2026) 193:68
https://doi.org/10.1007/s10955-026-03633-y

Spectral Prediction of Synchronization Clusters in Commuting Multilayer Networks

Sheida Ansarinasab[1] · Farnaz Ghassemi[1] · Fatemeh Parastesh[2,3] · Karthikeyan Rajagopal[2,4] · Sajad Jafari[1,5] · Matjaž Perc[6,7,8,9]

Received: 20 December 2025 / Accepted: 22 May 2026

Abstract

Cluster synchronization, where subsets of nodes evolve coherently while others remain desynchronized, underlies a wide range of coordinated phenomena in complex systems. In networks with multiple types of interactions—so-called hypernetworks—each coupling layer can promote distinct synchronization patterns, making it challenging to predict how coherent groups form and remain stable. Existing symmetry-based methods often require explicit group-theoretic identification, which becomes infeasible for large or structurally heterogeneous systems. Here, we introduce a spectral framework that predicts the hierarchical formation and stability of synchronization clusters in hypernetworks composed of commuting interaction layers. By exploiting the shared eigenspace of layer-specific Laplacian matrices, the framework analytically determines the sequence of cluster formation and decouples their stability via a generalized Master Stability Function. Numerical experiments with Chen and Lorenz oscillators confirm the theoretical predictions, revealing a one-to-one correspondence between spectral organization and the hierarchical emergence of synchronization clusters. This approach provides a unified, computationally efficient method for analyzing and controlling clustered coordination in systems governed by multiple, structurally compatible interaction mechanisms.

Keywords Hypernetworks · Cluster synchronization · Commuting Laplacians · Spectral analysis · Master Stability Function

1 Introduction

The study of complex networks, rooted in graph theory, has provided a powerful framework for understanding how structural connectivity influences collective dynamics in natural and engineered systems [1–3]. Network theory has enabled researchers to capture interdependence across scales—from neuronal assemblies [4–6] and economic systems [7, 8] to power grids [9, 10] and social interactions [11, 12]—by representing interacting components as nodes and their relations as edges. Within this context, synchronization has emerged as one

Communicated by Shin-ichi Sasa.

Extended author information available on the last page of the article

Published online: 07 June 2026

of the most fundamental and extensively studied collective behaviors [13–15]. It describes how dynamical units adjust their rhythms through mutual interaction, leading to coherent temporal evolution [13]. Beyond its conceptual importance, synchronization underlies essential real-world functions such as information processing in the brain [16, 17], coordination in sensor networks [18, 19], and stability in electrical grids [20, 21].

While early studies primarily focused on complete synchronization [13–15], where all nodes evolve identically, subsequent research has revealed that many natural systems exhibit far more intricate coordination patterns [22–24]. Depending on structural properties and coupling mechanisms, networks can display partial synchronization [23, 25], chimera states [22, 26], or hierarchical coordination patterns [24, 27]. Among these, cluster synchronization is one of the most significant and pervasive forms of collective behavior, in which nodes partition into distinct groups that maintain internal coherence while remaining desynchronized with other groups [28, 29]. This phenomenon captures a realistic middle ground between complete synchronization and total incoherence, reflecting the modular organization commonly observed in biological and technological networks [24, 30]. Understanding how such clusters emerge and remain stable is essential for uncovering the organizational principles that govern complex networked systems [27].

Numerous studies have investigated synchronization clusters and their stability under various conditions in networks composed of a single interaction layer [27, 29, 31]. For example, Bayani et al. showed that the progression toward complete synchronization in complex networks occurs through a sequence of cluster formations that can be predicted from the eigenvalues and eigenvectors of the graph Laplacian matrix [27]. Their spectral approach accurately identified the nodes forming each cluster and the coupling strengths at which they emerge, even in slightly heterogeneous networks. The study [31] introduced a spectral-block-based framework for controlling cluster synchronization in complex networks. By organizing Laplacian eigenvalues into localized spectral blocks, the authors demonstrated how to induce or eliminate clusters and control their synchronization sequence as coupling strength varies. Timofeyev and Patania (2025) further established a spectral framework linking almost equitable partitions (AEPs) to cluster synchronization [29]. By showing how Laplacian eigenvectors associated with AEPs govern synchronization cluster formation, they reduced network dynamics via quotient graph projections and extended the framework to quasi-equitable partitions for systems with structural imperfections, enabling the analysis of cluster synchronization in noisy or heterogeneous networks.

As research on networked systems has advanced, it has become clear that interactions in many real-world systems cannot be captured by a single-layer representation [32–34]. Entities often engage through multiple, functionally distinct couplings—for example, chemical and electrical synapses in neuronal systems [33], or social interactions encompassing friendships, collaborations, and online connections [34]. This recognition has motivated the development of the hypernetwork framework [35], in which each interaction layer represents a distinct coupling mechanism. Hypernetworks provide a more faithful depiction of systems characterized by diverse interaction types among entities [35]. While complete synchronization in hypernetworks has been studied extensively [32, 36, 37], cluster synchronization presents a greater analytical challenge due to the coexistence of multiple coupling mechanisms and heterogeneous topologies. Beyond identifying synchronization clusters, it is equally important to assess their dynamical stability. Analytical tools such as the Master Stability Function, MSF [38] offer a systematic means to evaluate local stability under the complex interplay of multiple interaction layers, providing both predictive insight and theoretical rigor.

In recent years, the analysis of cluster synchronization in multilayer and hypernetwork systems has drawn growing attention [28, 30, 39–41]. In 2019, Ma et al. examined synchronization clusters in multilayer networks through numerical simulations, exploring how interlayer coupling structures and correlations influence cluster formation and robustness [40]. Della Rossa et al. analyzed synchronization clusters by identifying symmetries both within and across layers using computational group theory [41], distinguishing independent layer symmetries (within a single layer) from dependent ones (spanning multiple layers). Their approach decomposed the dynamics into independent blocks and assessed stability via the MSF. Wang and Liu developed a geometrically motivated Lyapunov approach for cluster synchronization in multi-weighted and directed networks using pinning control, combining normalized left eigenvectors of multiple asymmetric coupling matrices to derive sufficient synchronization conditions [28]. The study [30] in 2024 investigated cluster synchronization in multilayer networks of delay-coupled semiconductor lasers, introducing disjoint layer symmetry to decouple stability across layers and expand the range of stable synchronization. More recently, synchronization clusters in phase-lagged multilayer networks of oscillators modeled by the Sakaguchi–Kuramoto dynamics were analyzed [39]. The authors showed that fully degree-correlated configurations—where oscillator frequencies align with network connectivity in both layers—significantly enhance the stability of cluster synchronization.

Despite notable advances in understanding complete synchronization in hypernetworks [32, 35–37], predicting the emergence and stability of synchronization clusters across multiple interaction layers remains a major challenge. Existing approaches based on computational group theory [30, 41] require explicit identification of all hypergraph symmetries in each layer, leading to prohibitive computational costs. To address this limitation, the present study introduces a spectral-based analytical framework that relies exclusively on the eigenvalues and eigenvectors of layer-specific Laplacian matrices. The novelty of the present work lies not in a direct extension of existing single-layer spectral methods, but in establishing a new framework for multilayer and hypernetwork systems under the commutativity condition. While previous spectral approaches have shown that Laplacian eigenvalues and eigenvectors can predict synchronization clusters in single-interaction networks [27, 29, 31], extending these ideas to multilayer systems is nontrivial due to the coexistence of multiple, generally incompatible spectral structures. Here, we show that when layer-specific Laplacian matrices commute, their shared eigenspace provides a unifying spectral backbone that simultaneously encodes the clustering architecture of all interaction layers. This enables, for the first time, the analytical prediction of the entire hierarchical sequence of synchronization cluster formation across multiple layers using a single orthogonal basis. Moreover, the framework yields a fully decoupled MSF for all clusters without resorting to explicit symmetry detection, group-theoretic analysis, or layer-by-layer quotient graph constructions. As such, the proposed approach establishes a distinct and scalable spectral paradigm for analyzing cluster synchronization in structurally compatible multilayer networks.

2 Methodological Framework

In this section, we present a comprehensive overview of the mathematical formulations describing the hypernetworks examined in this study, along with an analytical approach for predicting the sequence of synchronization cluster formation and assessing their stability using a decoupled MSF framework.

2.1 Hypernetworks Mathematical Description

In a hypernetwork composed of N identical oscillators and M distinct interaction layers, the temporal dynamics of the i th oscillator can be expressed based on the following relations.

$$\dot{X}_i = F(X_i) + \sum_{\alpha=1}^{M} \sigma_\alpha \sum_{j=1}^{N} A^\alpha{}_{ij} G^\alpha(X_i, X_j), \quad i = 1, 2, \ldots, N. \tag{1}$$

In Eq. 1, $X_i = (x_{i1}, x_{i2}, \ldots, x_{in})^T$ denotes the n-dimensional state vector of the i th oscillator. The vector functions $F : R^n \to R^n$ and $G^\alpha : R^n \times R^n \to R^n$ describe, respectively, the intrinsic dynamics of isolated oscillators and the coupling mechanism among them through the interaction layer α associated with the coupling strength σ_α. The $N \times N$ adjacency matrix A^α represents the connectivity pattern of the graph related to the interaction layer α. In the present study, the hypernetworks under consideration comprise undirected and weighted graphs. Consequently, each adjacency matrix A^α is symmetric, and the entry $A^\alpha{}_{ij} = A^\alpha{}_{ji}$ specifies the weight of the edge connecting nodes i and j through the layer α in the hypernetwork. Corresponding to each adjacency matrix A^α, the Laplacian matrix L^α is defined as $L^\alpha = D^\alpha - A^\alpha$, where $\sum_{j=1}^{N} L^\alpha{}_{ij} = 0$ for $i = 1, 2, \ldots, N$. The diagonal degree matrix D^α contains the node degrees through the interaction layer α, with diagonal entries $D^\alpha{}_{ii} = \sum_{j=1}^{N} A^\alpha{}_{ij}$ for $i = 1, 2, \ldots, N$. Hence, the hypernetwork described by Eq. 1 can equivalently be reformulated in terms of the Laplacian matrices L^α and the differential coupling functions $G^\alpha\big(X_i, X_j\big) = G^\alpha(X_j) - G^\alpha(X_i)$ as expressed in Eq. 2.

$$\dot{X}_i = F(X_i) - \sum_{\alpha=1}^{M} \sigma_\alpha \sum_{j=1}^{N} L^\alpha{}_{ij} G^\alpha\big(X_j\big), \quad i = 1, 2, \ldots, N. \tag{2}$$

Such a representation establishes the foundation for analyzing synchronization patterns and cluster formation in hypernetworks within a unified spectral framework.

2.2 Hypernetworks Structural Features

The present study aims to predict the sequence of synchronization clusters and analyze their stability in the hypernetworks described by Eqs. 1 and 2, based on the common eigenspace of the Laplacian matrices of different interaction layers. Accordingly, the graphs corresponding to the various interaction layers exhibit a clustered structure, with their respective Laplacian matrices being simultaneously pairwise diagonalizable. The following subsections provide a detailed description of the structural features of these graphs and the methodology used to construct them.

2.2.1 Clustering Architecture

The graphs corresponding to the various interaction layers that constitute the hypernetworks examined in this study exhibit a clustered organization characterized by a *strong equitable* type. In general, for each graph of the hypernetwork described by the adjacency matrix A^α, a partition of the node set $V = \{1, 2, 3, \ldots, N\}$ into K disjoint clusters $C_1{}^\alpha, C_2{}^\alpha, \ldots, C_K{}^\alpha$ is said to be *external equitable* if, for every pair of clusters $\big(C_p{}^\alpha, C_q{}^\alpha\big) p \neq q$, each node $i \in C_p{}^\alpha$ has the same total edge weight from the nodes in $C_q{}^\alpha$ [27]. Mathematically, this condition can be expressed as Eq. 3.

$$\sum_{j \in C_q{}^\alpha} A^\alpha{}_{ij} = \gamma^\alpha{}_{pq}, \quad \forall i \in C_p{}^\alpha, \quad p \neq q, \quad \alpha = 1, 2, \ldots, M, \tag{3}$$

where $\gamma^\alpha{}_{pq}$ denotes the inter-cluster connection weight from cluster C_q to cluster C_p through the interaction layer α.

A *strong equitable* partition is a special form of an *external equitable* partition in which all nodes within a cluster are indistinguishable from the perspective of nodes outside that cluster [27]. In other words, each node outside a given cluster is connected to all nodes within that cluster with the same edge weight or is not connected to any of them. So, for every cluster $C_p{}^\alpha$, the following condition holds.

$$A^\alpha{}_{ij} = A^\alpha{}_{i\prime j} \quad \forall i, i\prime \in C_p{}^\alpha, \quad \forall j \in V \backslash C_p{}^\alpha, \quad \alpha = 1, 2, \ldots, M. \tag{4}$$

Equation 4 implies that all nodes within the same cluster have identical external degree, meaning they receive the same total input from the rest of the graph. Notably, in a *strong equitable* partition, the internal connections among nodes within each cluster are irrelevant; therefore, the clusters are not necessarily symmetric orbits. Symmetry, in this context, refers to a structural equivalence in which nodes can be interchanged without affecting the graph's overall connectivity pattern [27].

2.2.2 Simultaneously Diagonalizable Laplacians

The Laplacian matrix L^α of the interaction layer α in the hypernetwork described by Eq. 2, encapsulates the connectivity and nodal degree information of the adjacency matrix A^α according to the definition provided in the preceding subsections. Since this work aims to analyze the stability of all synchronization clusters based on the decoupled MSF, the Laplacian matrices of different interaction layers in the hypernetwork are assumed to be pairwise commuting, allowing them to be simultaneously diagonalizable. It is worth noting that, in the present study, all Laplacians are symmetric because the graphs related to the interaction layers are undirected, which is crucial for the following properties. Mathematically, a set of symmetric Laplacians $\left\{L^1, L^2, \ldots, L^M\right\}$ is pairwise commuting (thus simultaneously diagonalizable) if, for any pair (L^i, L^j), there exists a common invertible matrix P such that,

$$P^{-1} L^i P = \Lambda^i, \quad P^{-1} L^j P = \Lambda^j, \quad i, j = 1, 2, \ldots, M \quad i \neq j, \tag{5}$$

where Λ^i and Λ^j are diagonal matrices containing the eigenvalues of L^i and L^j, respectively.

Two distinct methods, including (I) common eigenbasis and (II) functional mapping are employed in the present study to construct symmetric commuting Laplacians [42, 43]. In approach I [42], first, a Laplacian L^i is diagonalized as $P_i{}^{-1} L^i P_i = \Lambda^i$. The Laplacian of another layer, L^j, is then constructed in the same eigenbasis by choosing a new diagonal matrix $\Lambda^j = diag(\mu_1, \mu_2, \mu_3, \ldots, \mu_N)$, where $\mu_1 = 0$ to satisfy the zero-row-sum property, and the remaining positive eigenvalues $\{\mu_2, \mu_3, \ldots, \mu_N\}$ are sorted in the same order as those of Λ^i. The new Laplacian is then formed as $L^j = P_i \Lambda^j P_i{}^{-1}$. This ensures that L^i and L^j share the same eigenvectors and are therefore simultaneously diagonalizable. In approach II [43], L^j can be defined as a nonlinear function of L^i, i.e., $L^j = H(L^i)$, where the function H is designed to preserve diagonalizability in the eigenbasis of L^i. In both methods, additional constraints, including symmetry, zero row sums, and non-positive off-diagonal elements, are imposed to guarantee that the resulting matrices retain the defining characteristics of valid Laplacians and are suitable for network dynamical analysis.

Moreover, since all constructed Laplacians are symmetric and pairwise commuting, they are orthogonally simultaneously diagonalizable. Therefore, there exists at least one orthogonal matrix Q (i.e., a matrix satisfying $QQ^T = Q^T Q = I_N$) that simultaneously diagonalizes all Laplacians of different interaction layers as follows.

$$Q^T L^\alpha Q = \Lambda^\alpha \quad \forall\alpha = 1, 2, \dots, M. \tag{6}$$

In Eq. 6, Λ^α is the diagonal matrix of eigenvalues related to the interaction layer α. This property preserves the Laplacian clustering structures and provides a mathematically rigorous foundation for defining common eigenmodes across all interaction layers in the hypernetwork.

It is worth noting that the commutativity condition imposed on the interaction layers of the hypernetwork ensures that, although the corresponding Laplacian matrices are distinct, they share an identical clustering structure. In other words, the best partitioning of the hypernetwork nodes that yields the minimum number of different strong equitable clusters is the same across all individual interaction layers [44].

2.3 Synchronization Clusters Prediction

In 2024, Bayani et al. [27] conducted a study to predict the entire sequence of synchronization cluster formation leading to complete synchronization in single-interaction networks. In their work, the authors demonstrated that it is possible to predict both the sequence of emerging synchronization clusters and the corresponding coupling strengths solely based on the eigenvectors and eigenvalues of the network's Laplacian matrix. In the present study, we extend the approach proposed in [27] to predict the entire sequence of synchronization cluster formation in hypernetworks described by Eq. 2. As explained in the previous subsections, the Laplacian matrices associated with the different interaction layers of these hypernetworks are pairwise commutative and can be simultaneously diagonalized by an orthogonal matrix Q. Consequently, the clustering properties of all interaction layers are embedded in matrix Q, which represents the common eigenbasis of different Laplacians in the hypernetworks.

Each column q_i of the orthogonal matrix $Q = [q_1, q_2, \dots, q_N]$ corresponds to the i th shared eigenvector of all layer-specific Laplacians L^α, satisfying the following relation.

$$L^\alpha q_i = {\mu_i}^\alpha q_i, \quad \alpha = 1, 2, \dots, M. \tag{7}$$

Thus, based on Eq. 7, for each q_i an M-tuple of eigenvalues $\boldsymbol{\mu_i} = ({\mu_i}^1, {\mu_i}^2, \dots, {\mu_i}^M)$ is obtained, which characterizes the spectral response of the i th eigenmode across all interaction layers of the hypernetwork. As the coupling strengths $(\sigma_1, \sigma_2, \dots, \sigma_M)$ between oscillators gradually increase from zero, the hypernetwork successively exhibits the emergence and merging of the synchronization clusters, leading to the complete synchronization of the hypernetwork. Assuming that the synchronization manifolds corresponding to different clusters do not deviate significantly from the complete synchronization manifold, the orthogonal matrix Q can be used to predict the entire sequence of synchronization cluster formation in the hypernetwork. It is noteworthy that, as stated in [27], the proposed algorithm is valid only for coupling functions that vanish on the synchronization manifold of the hypernetwork. Under this condition, the synchronization manifold of the hypernetwork follows the same dynamics as that of uncoupled oscillators.

In the first step of implementing the generalized algorithm proposed in the present study, the orthogonal matrix $Q = [q_1, q_2, \ldots, q_N]$ is considered as follows.

$$Q = \begin{bmatrix} q_{11} & q_{21} & \cdots & q_{N1} \\ q_{12} & q_{22} & \cdots & q_{N2} \\ \vdots & \vdots & \ddots & \vdots \\ q_{1N} & q_{2N} & \cdots & q_{NN} \end{bmatrix}.$$

For each M-tuple of eigenvalues $\boldsymbol{\mu_i} = ({\mu_i}^1, {\mu_i}^2, \ldots, {\mu_i}^M)$ corresponding to the i th common eigenvector q_i (see Eq. 7), a symmetric matrix $E_{\boldsymbol{\mu}_i}$ with zero diagonal elements is constructed as outlined below.

$$E_{\boldsymbol{\mu}_i} = \begin{bmatrix} (q_{\mathrm{i}1} - q_{\mathrm{i}1})^2 & (q_{\mathrm{i}2} - q_{\mathrm{i}1})^2 & \ldots & (q_{\mathrm{iN}} - q_{\mathrm{i}1})^2 \\ (q_{\mathrm{i}1} - q_{\mathrm{i}2})^2 & (q_{\mathrm{i}2} - q_{\mathrm{i}2})^2 & \ldots & (q_{\mathrm{iN}} - q_{\mathrm{i}2})^2 \\ \vdots & \vdots & \ddots & \vdots \\ (q_{\mathrm{i}1} - q_{\mathrm{iN}})^2 & (q_{\mathrm{i}2} - q_{\mathrm{iN}})^2 & \ldots & (q_{\mathrm{iN}} - q_{\mathrm{iN}})^2 \end{bmatrix}.$$

Without loss of generality, let the matrices $E_{\boldsymbol{\mu}_i}$ $(i = N, N-1, \ldots, 1)$ correspond to the M-tuple of eigenvalues ordered from the largest to the smallest. Then, the sequence of synchronization clusters formation in the hypernetwork, consisting of N stages, is predicted from the ordered set of matrices $\{S_i\}_{i=N}^{i=1}$ as follows.

$$\begin{aligned} S_N &= E_{\boldsymbol{\mu}_N}, \\ S_{N-1} &= S_N + E_{\boldsymbol{\mu}_{N-1}}, \\ &\vdots \\ S_2 &= S_3 + E_{\boldsymbol{\mu}_2}, \\ S_1 &= S_2 + E_{\boldsymbol{\mu}_1}. \end{aligned}$$

Each element of the matrix S_n related to the stage $N - n + 1$ of the clustering sequence is calculated based on Eq. 8.

$$(S_n)_{kl} = \sum_{i=n}^{N} (q_{ik} - q_{il})^2 \tag{8}$$

here, q_{ik} and q_{il} denote the k th and l th elements of the i th column of matrix Q, respectively. The matrix Q is orthogonal, so its rows also form an orthonormal basis for the space R^N. Accordingly, each element $(S_n)_{kl}$ is precisely the sum of squared differences of the last $N - n + 1$ components of the vectors related to the k th and l th row of matrix Q. Because these rows are orthonormal, the maximum possible value of any element in the symmetric matrix S_n is two, corresponding to the squared Euclidean distance between two orthonormal vectors.

At each stage $N-n+1$ of the clustering sequence, the indices of the elements in the matrix S_n that form a block of entries equal to two correspond to the nodes of the hypernetwork that constitute a cluster. Also, multiple distinct blocks of entries with values equal to two may appear in the matrix S_n, each represents a separate cluster that coexists with others within the hypernetwork. As the clustering sequence progresses from its initial to its final stages, various synchronization clusters within the hypernetwork gradually merge, forming larger clusters. Ultimately, at the stage $N-1$ of the clustering sequence corresponding to the matrix S_2, all oscillators in the hypernetwork form a single synchronization cluster, indicating the emergence of complete synchronization. Let cluster C at stage $N - n + 1$ of the clustering sequence, according to the matrix S_n, consist of m nodes with indices 1,2, ..., m without loss of generality. This cluster corresponds to a block B_C of dimension $N \times (m-1)$, composed of $(m-1)$ columns (eigenvectors) of the orthogonal matrix Q. In all these eigenvectors, only the components corresponding to the indices of the cluster nodes are nonzero, while all other components are zero. Conversely, each of the remaining eigenvectors outside this block exhibits identical values across the entries corresponding to the indices of the cluster nodes. According to Eq. 8, for any two nodes k and l belonging to the same cluster C ($k, l = 1,2, \ldots, mk \neq l$), only the columns of Q contained within the block B_C contribute to the value of the element $(S_n)_{kl}$. In essence, the eigenvectors forming the block B_C represent directions orthogonal to the synchronization manifold of cluster C and play a critical role in determining the stability of this synchronization cluster. Finally, based on Eq. 7, the set of $(m-1)M$-tuples $\boldsymbol{\mu_{ci}} = ({\mu_{ci}}^1, {\mu_{ci}}^2, \ldots, {\mu_{ci}}^M)$ associated with each eigenvector q_i in the block B_C can be computed. These eigenvalue tuples characterize the spectral components that govern the stability of the synchronization manifold corresponding to cluster C.

2.4 Stability Analysis of Synchronization Clusters

In this subsection, we analyze the stability of synchronization clusters in the hypernetwork by extending the MSF approach [38]. This approach provides a powerful analytical tool to determine the local stability of synchronized states by decoupling the network dynamics from the coupling structure. It is worth noting that the stability analysis of complete synchronization for single-interaction networks using the MSF framework is provided in "Appendix".

Without loss of generality, we focus on a specific cluster C of the hypernetwork, consisting of m nodes with indices $i = 1, 2, \ldots, m$. The dynamics of the i th node in the cluster C, considering its connections with other nodes both within and out of the cluster, can be described by Eq. 9.

$$\dot{X}_i = F(X_i) - \sum_{\alpha=1}^{M} \sigma_\alpha \left(\sum_{j \in C} {L^\alpha}_{ij} G^\alpha\left(X_j\right) + \sum_{j \notin C} {L^\alpha}_{ij} G^\alpha\left(X_j\right) \right), \quad i = 1, 2, \ldots, m. \tag{9}$$

Since the diagonal elements of the Laplacian matrices L^α do not contribute to the term $\sum_{j \notin C} {L^\alpha}_{ij} G^\alpha\left(X_j\right)$, Eq. 9 can be rewritten in the simplified form of Eq. 10.

$$\dot{X}_i = F(X_i) - \sum_{\alpha=1}^{M} \sigma_\alpha \left(\sum_{j \in C} {L^\alpha}_{ij} G^\alpha\left(X_j\right) - \sum_{j \notin C} {A^\alpha}_{ij} G^\alpha\left(X_j\right) \right), \quad i = 1, 2, \ldots, m. \tag{10}$$

In Eq. 10, the coupling term $\sigma_\alpha \sum_{j \notin C} {A^\alpha}_{ij} G^\alpha\left(X_j\right)$ represents the total input received by the ith node of cluster C in interaction layer α from the rest of the network corresponding to that layer. Because the clusters in all interaction layers of the hypernetwork are assumed to be strong equitable clusters, this coupling term is identical for all nodes within the cluster C and is independent of i. Under the condition of synchronization for cluster C, all nodes in C evolve toward the synchronization manifold defined as $X_1 = X_2 = \ldots = X_m = X_{sc}$. The dynamics of all nodes within the cluster C in the synchronized state are governed by Eq. 11.

$$\dot{X}_{sc} = F(X_{sc}) - \sum_{\alpha=1}^{M} \sigma_\alpha \left(G^\alpha(X_{sc}) \sum_{j \in C} L^\alpha{}_{ij} - \sum_{j \notin C} A^\alpha{}_{ij} G^\alpha\left(X_j\right) \right), \quad i = 1, 2, \ldots, m. \tag{11}$$

In Eq. 11, the term $d_c{}^\alpha = \sum_{j \in C} L^\alpha{}_{ij}$ equals the total weight of edges between the node i in the cluster C of interaction layer α and all other nodes outside the cluster in that layer, which is identical for all nodes belonging to the same cluster. Consequently, the equation describing the synchronized state dynamic for cluster C can be expressed as Eq. 12.

$$\dot{X}_{sc} = F(X_{sc}) - \sum_{\alpha=1}^{M} \sigma_\alpha \left(d_c{}^\alpha G^\alpha(X_{sc}) - \sum_{j \notin C} A^\alpha{}_{ij} G^\alpha\left(X_j\right) \right), \quad i = 1, 2, \ldots, m. \tag{12}$$

According to Eq. 12, it can be observed that the synchronization manifold of cluster C, unlike the complete synchronization manifold of the entire hypernetwork, does not solely depend on the intrinsic dynamics of the isolated oscillators ($\dot{X}_{sc} = F(X_{sc})$). In fact, the synchronization manifold of each cluster in the hypernetwork is influenced by the entire hypernetwork dynamics, the coupling functions G^α of different interaction layers, and the set of coupling strengths $(\sigma_1, \sigma_2, \ldots, \sigma_M)$. Moreover, the coupling strength sets that lead to the formation of synchronization clusters in the clustering sequence, and also the d^α are not identical for different clusters of the hypernetwork. Therefore, the synchronization manifolds corresponding to different clusters are also distinct.

Nevertheless, there are two main reasons to assume that the synchronization manifold of each cluster approximately follows the intrinsic dynamics of the isolated oscillators in the hypernetwork, i.e. $\dot{X}_{sc} = F(X_{sc})$. First, for analyzing the sequential formation of synchronization clusters in the hypernetwork, the coupling strengths $(\sigma_1, \sigma_2, \ldots, \sigma_M)$ gradually increase from zero, and their values generally remain within a moderate range, far from large magnitudes. Second, as indicated by Eq. 12, in the stability analysis of synchronization cluster C, no explicit constraints are imposed on the dynamics of nodes outside the cluster across the different interaction layers. Consequently, the second term of Eq. 12 consists of independent components whose combined contribution remains relatively small. Therefore, it can be approximated that this term has a negligible value for all synchronization clusters in the hypernetwork, implying that the synchronization manifold of each cluster approximately follows the isolated oscillator dynamics.

To analyze the local stability of the synchronization manifold of cluster C, slight deviations of the form $\delta X_i = X_i - X_{sc}$ are considered for each node i belonging to cluster C. Linearizing Eq. 10 around the X_{sc} yields the deviation dynamics for node i of cluster C, as expressed in Eq. 13.

$$\delta\dot{X}_i = DF(X_{sc})\delta X_i - \sum_{\alpha=1}^{M} \sigma_\alpha \sum_{j \in C} L^\alpha{}_{ij} DG^\alpha(X_{sc})\delta X_j, \quad i = 1, 2, \ldots, m. \tag{13}$$

In Eq. 13, the $n \times n$ matrices DF and DG^α represent the Jacobian matrices of vector functions F and G^α evaluated at the synchronization manifold X_{sc} of cluster C. By stacking the deviation vectors of all cluster nodes as $\delta X = [\delta X_1{}^T, \delta X_2{}^T, \ldots, \delta X_m{}^T]^T$ and employing the Kronecker product $\otimes$, the collective deviation dynamics of cluster C from its synchronization manifold can be compactly written as Eq. 14.

$$\delta\dot{X} = (I_m \otimes DF(X_{sc}) - \sum_{\alpha=1}^{M} \sigma_\alpha ({L_c}^\alpha + {d_c}^\alpha I_m) \otimes DG^\alpha(X_{sc}))\delta X. \tag{14}$$

In Eq. 14, I_m denotes the $m \times m$ identity matrix. The ${L_c}^\alpha$ with dimension $m \times m$ represents the Laplacian matrix associated with the block of m nodes in the hypernetwork forming cluster C in layer α, and satisfies $\sum_{j=1}^{m} {L_{cij}}^\alpha = 0, i = 1,2, \ldots, m$.

Since the symmetric Laplacians L^α of different interaction layers α are pairwise commutative, the corresponding symmetric intra-cluster Laplacians ${L_c}^\alpha$ for cluster C are likewise pairwise commutative. Hence, there exists an orthogonal matrix $Q_c \in R^{m\times m}$ that simultaneously diagonalizes the Laplacians $\{{L_c}^\alpha\}_{\alpha=1}^{M}$. The orthogonal matrix Q_c can be chosen to reflect the natural decomposition into the synchronization manifold direction and its orthogonal complement for cluster C as $Q_c = [O\prime_{m\times 1} O_{m\times(m-1)}]$. The m-dimensional vector $O\prime = \frac{1}{\sqrt{m}}[1,1, \ldots, 1]^T$ lies along the synchronization manifold of cluster C. As described in Sect. 2.3, let the columns of the matrix B_C with dimension $N \times (m-1)$ represent the common eigenvectors of the orthogonal matrix Q associated with the synchronization cluster C. The matrix O is then obtained by extracting, from all the columns of B_C, the m nonzero elements corresponding to the indices of the nodes that form cluster C. By premultiplying Eq. 14 by ${Q_c}^T \otimes I_n$ and defining the new variable as $\eta = ({Q_c}^T \otimes I_n)\delta X$, m decoupled equation, each with dimension $n \times 1$ is obtained, as expressed in Eq. 15.

$$\dot{\eta}_i = \left(DF(X_{sc}) - \sum_{\alpha=1}^{M} \sigma_\alpha \left({\lambda_{ci}}^\alpha + {d_c}^\alpha\right) DG^\alpha(X_{sc})\right)\eta_i, \quad i = 1, 2, \ldots, m. \tag{15}$$

In Eq. 15, the term ${\mu_{ci}}^\alpha = {\lambda_{ci}}^\alpha + {d_c}^\alpha$ represents the sum of the i th eigenvalue of the Laplacian matrix ${L_c}^\alpha$ associated with cluster C (${\lambda_{ci}}^\alpha$) and the external degree of the cluster nodes (${d_c}^\alpha$) in the interaction layer α. The MSF is defined as the largest Lyapunov exponent (LLE) of Eq. 15, expressed as an M-dimensional function of the parameters $\boldsymbol{\zeta_{ci}} = (\sigma_1 {\mu_{ci}}^1, \sigma_2 {\mu_{ci}}^2, \ldots, \sigma_M {\mu_{ci}}^M)$ for $i = 1, 2, \ldots, m$. The M-tuple $\boldsymbol{\mu_{c1}} = ({d_c}^1, {d_c}^2, \ldots, {d_c}^M)$ corresponds to the common eigenvector $O\prime_{m\times 1}$, which lies along the synchronization manifold of cluster C and therefore does not influence its synchronization stability. The remaining M-tuples $\boldsymbol{\mu_{ci}}$ for $i = 2, 3, \ldots, m$ correspond to the common eigenvectors orthogonal to the synchronization manifold of the cluster and play a crucial role in determining its stability in the hypernetwork. It is worth noting that these M-tuples ($\boldsymbol{\mu_{ci}}$ for $i = 2, 3, \ldots, m$) obtained from the decoupled MSF equations for cluster C are identical to those determined through the method introduced in Sect. 2.3. The synchronous state of cluster C is considered locally stable if the maximum of the LLEs associated with Eq. 15 for $i = 2, \ldots, m$ is negative, implying that the deviation amplitudes from the cluster's synchronization manifold asymptotically decay to zero over time.

3 Results

This section provides a detailed explanation of the simulation results, focusing on the analysis of synchronization clusters and their stability in networks composed of multiple interaction layers with commuting Laplacian matrices. In the present study, to numerically evaluate the synchronization within cluster C consisting of m nodes of the hypernetwork with indices $i =$

$1, 2, \ldots, m$, the cluster synchronization error (CE) criterion defined in Eq. 16 is employed [27].

$$CE = \left\langle \frac{1}{m} \sum_{i=1}^{m} \|X_i(t) - \overline{X}_c(t)\| \right\rangle_t . \quad (16)$$

In Eq. 16, $X_i(t)$ denotes the n-dimensional state variable vector of the i th oscillator in the cluster C at time$t$. The $\overline{X}_c(t)$ represents the average of the state variable vectors of all oscillators in cluster$C$, obtained according to the relation$\overline{X}_c(t) = \frac{1}{m}\sum_{i=1}^{m} X_i(t)$. The symbols $\|.\|$ and $\langle . \rangle_t$ denote the Euclidean norm and time averaging, respectively. The CE criterion quantifies the degree of coherence among the oscillators within the cluster. Therefore, a smaller value of CE indicates a higher level of synchronization among the oscillators in the cluster, and vice versa. In all simulations of the present study, the CE is computed after discarding an initial transient of $t = 800$ time units to ensure convergence to the asymptotic dynamical regime, and it is then averaged over the time window$t \in [800, 1000]$. A cluster is classified as synchronized if its CE falls below a fixed numerical threshold of10^{-3}, which robustly distinguishes between synchronized and desynchronized states across all coupling parameter values considered.

To provide a more precise visualization of the simulation results obtained from the theoretical framework presented in Sect. 2, this study examines hypernetworks comprising two distinct interaction layers. To construct commuting Laplacian matrices within these hypernetworks, a weighted, undirected, and fully connected base graph with adjacency matrix B including ten nodes, corresponding to one of the two interaction layers, is considered, as illustrated in Fig. 1. As shown in this figure, the nodes of graph B are divided into three strong equitable clusters, including cluster 1 with nodes (1, 2, 3), cluster 2 with nodes (4, 5, 6), and cluster 3 with nodes (7, 8, 9, 10). As demonstrated by the adjacency matrix B of the graph shown in Fig. 1b, each node outside a strong equitable cluster is connected to all nodes in the cluster with identical edge weights, while the connections among the nodes within the cluster differ. Consequently, the clusters are not the symmetry orbits of the graph. It is noteworthy that the Laplacian matrix of graph B possesses nine distinct nonzero eigenvalues. Subsequently, the graphs for the other interaction layer in different hypernetworks are constructed using the procedures described in Sect. 2.2.2.

The following subsections present a detailed analysis of the results concerning the synchronization clusters in hypernetworks composed of Chen and Lorenz oscillators. All simulations in the present study are performed using the fourth-order Runge–Kutta method [45], with a total runtime of $T = 1000$ and time steps of $dt = 0.003$ and $dt = 0.005$ for hypernetworks composed of Chen and Lorenz oscillators, respectively. Also, all simulations are repeated under 100 different random initial conditions in the interval of $[-10, 10]$ to ensure the reliability of the results.

3.1 Synchronization Clusters Analysis in the Hypernetwork Composed of Chen Systems

This subsection presents the results from analyzing synchronization clusters and their stability in the hypernetwork composed of Chen systems. To this end, the graph shown in Fig. 1 is considered to describe the connectivity among the nodes of the hypernetwork in the first interaction layer ($A^1 = B$). The graph of the second interaction layer with the adjacency matrix A^2

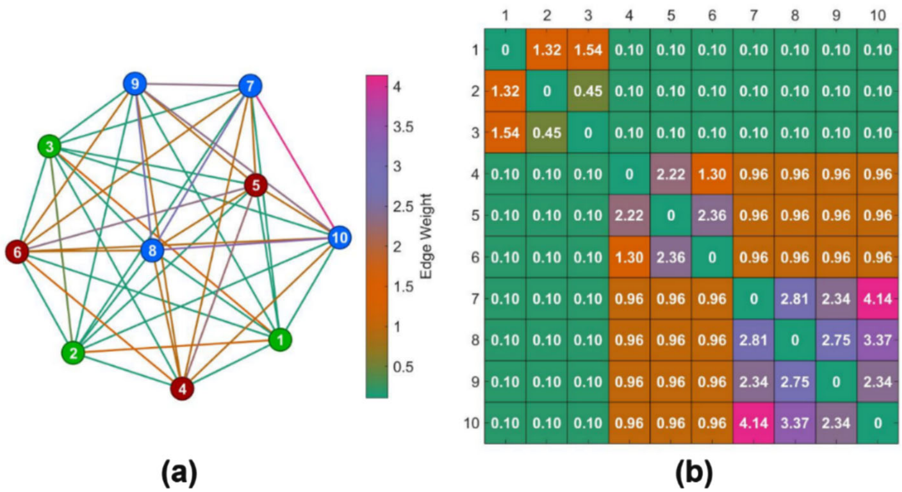

Fig. 1 The diagrams of **a** the weighted and undirected base graph considered for one of the two interaction layers of the hypernetworks examined in this study, and **b** the corresponding adjacency matrix B. This graph consists of ten nodes, represented by solid colored circles. The edge weights connecting the graph nodes and the corresponding elements in the adjacency matrix are shown using the color bar, with each edge weight assigned the same color as its corresponding element in the adjacency matrix. As illustrated in panels **a** and **b**, the nodes of this graph are divided into three strong equitable clusters. The first cluster comprises nodes 1–3, represented in green; the second cluster includes nodes 4–6, depicted in red; and the third cluster comprises nodes 7–10, represented in blue. As shown, each node outside a cluster is connected to all nodes within the cluster, with identical edge weights

is then constructed using the common eigenbases method described in Sect. 2.2.2. The intrinsic dynamics of the uncoupled oscillators in the hypernetwork follow the three-dimensional Chen system defined by the function $F(X) = (a(y-x), (c-a-z)x + cy, xy - \beta z)^T$, where $X \equiv (x, y, z)^T$. In the Chen system, the parameters $a = 35$, $c = 28$, and $\beta = 8/3$ are selected to ensure chaotic behavior [46].

In general, the coupling functions associated with each interaction layer α in the hypernetworks of the present study are considered to be linear-diffusive $G^{\alpha}\left(X_j\right) = g^{\alpha} X_j$, where g^{α} is an $n \times n$ coupling matrix with binary elements (0 or 1). An element ${g^{\alpha}}_{ij} = 1$ indicates that the difference between the j th state variables of two oscillators is fed back as a coupling term into the i th state variable equation of the oscillator. In the hypernetwork examined in this subsection, the couplings between oscillators in the first and second interaction layers are defined by the following coupling matrices:

$$g^1 = \begin{bmatrix} 0 & 0 & 0 \\ 1 & 0 & 0 \\ 0 & 0 & 0 \end{bmatrix}, g^2 = \begin{bmatrix} 0 & 0 & 0 \\ 0 & 1 & 0 \\ 0 & 0 & 0 \end{bmatrix}.$$

After applying the proposed method introduced in Sect. 2.3 to the orthogonal matrix Q, which simultaneously diagonalizes the Laplacian matrices corresponding to graphs A^1 and A^2 as described in Eq. 7, the obtained results are summarized in Table 1. The first and second columns of Table 1 present the nodes constituting the clusters and the corresponding stages in the predicted clustering sequence at which the related synchronization clusters emerge, respectively. According to this table, the third strong equitable cluster, composed of nodes

Table 1 The predicted sequence of synchronization clusters formation in hypernetworks composed of Chen and Lorenz systems

Cluster nodes	Existence	Related pairs of eigenvalues	
		Hypernetwork with Chen oscillators $(\mu_c{}^1, \mu_c{}^2)$	Hypernetwork with Lorenz oscillators $(\mu_c{}^1, \mu_c{}^2)$
(7, 8, 9, 10)	Stages 3 to 5	(17, 19), (15, 17), (13, 15)	(12.77, 17), (11.47, 15), (10.15, 13)
(4, 5, 6)	Stage 5	(11, 13), (9, 11)	(8.82, 11), (7.48, 9)
(4, 5, 6, 7, 8, 9, 10)	Stages 6 to 8	(17, 19), (15, 17), (13, 15) (11, 13), (9, 11), (7, 9)	(12.77, 17), (11.47, 15), (10.15, 13) (8.82, 11), (7.48, 9), (6.11, 7)
(1, 2, 3)	Stage 8	(5, 7), (3, 5)	(4.71, 5), (3.24, 3)

The first and second columns indicate the indices of oscillators forming each predicted synchronization cluster and the corresponding stages in the clustering sequence where that cluster appears. The third and fourth columns present the pairs of eigenvalues associated with the eigenvectors orthogonal to the synchronization manifold of each cluster in the hypernetwork

7–10, is the first synchronization cluster to appear at the third stage of the clustering sequence. This synchronization cluster persists through the fourth and fifth stages. In addition to this cluster in the fifth stage, the second strong equitable cluster, comprising nodes 4–6, emerges independently. Subsequently, these two clusters merge at the sixth stage to form a larger synchronization cluster containing nodes 4 through 10. This large cluster remains intact during the seventh and eighth stages of the clustering sequence. In the eighth stage, the first strong equitable cluster, consisting of nodes 1–3, also arises. Finally, at the ninth stage of the clustering sequence, this cluster merges with the larger cluster, resulting in complete synchronization within the hypernetwork. Furthermore, Table 1 lists, for each predicted synchronization cluster, the corresponding pairs of eigenvalues $(\mu_c{}^1, \mu_c{}^2)$ associated with the eigenvectors orthogonal to the synchronization manifold of the cluster, which play a key role in assessing the cluster stability.

In the following, to provide a better illustration of the synchronization clusters formation sequence within the hypernetwork of Chen systems, the coupling strength related to the first interaction layer is fixed at $\sigma_1 = 0.36$, while the coupling strength corresponding to the other interaction layer σ_2 is varied. Then, the state variable x of all oscillators at the final time point of the simulations ($t = 1000$) is plotted for those σ_2 values corresponding to the first appearance of the synchronization clusters reported in Table 1, as depicted in Fig. 2.

Panel (a) of Fig. 2 illustrates that the synchronization cluster composed of oscillators 7–10 (the third strong equitable cluster) in the hypernetwork emerges for the first time at the small coupling strength $\sigma_2 = 0.19$. This cluster remains the only synchronization cluster within the hypernetwork until σ_2 reaches 0.29, as shown in panel (b), where an additional synchronization cluster comprising oscillators 4–6 (the second strong equitable cluster) appears for the first time. As depicted in panel (c), further increasing σ_2 to 0.41 causes the previously formed clusters to merge, resulting in a larger synchronization cluster that includes oscillators 4 through 10 of the hypernetwork. Finally, at $\sigma_2 = 0.81$, the first strong equitable cluster consisting of oscillators 1–3 emerges alongside the cluster of oscillators 4 to 10. Notably, as σ_2 increases further to 1.4, complete synchronization among all oscillators in the hypernetwork is achieved.

In what follows, Fig. 3 illustrates the synchronization error of the predicted clusters in the

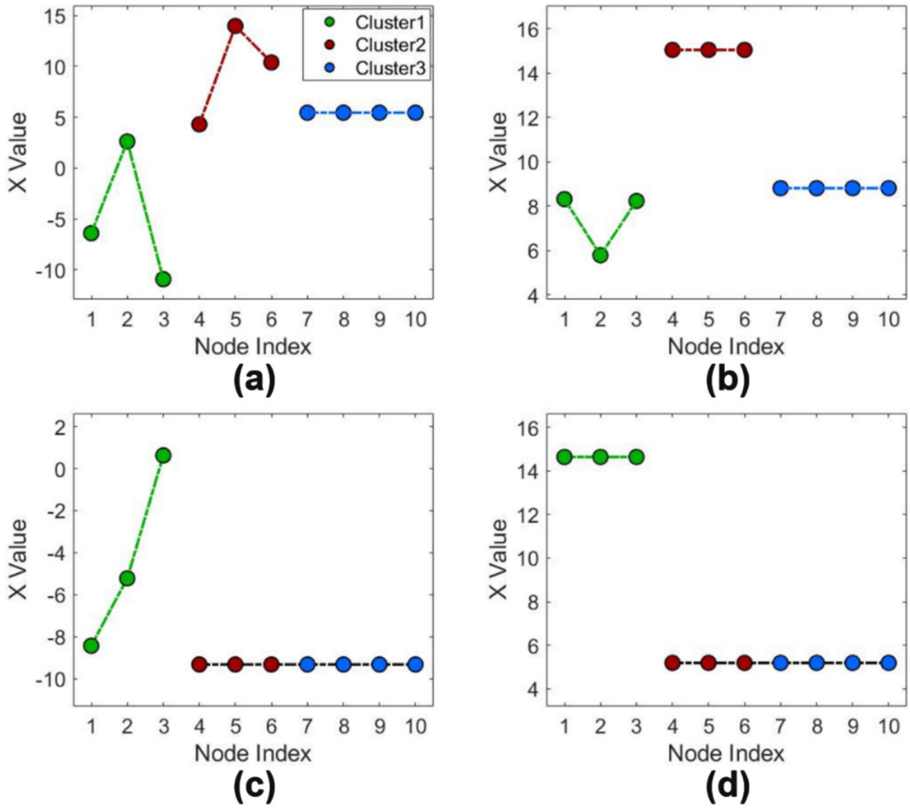

Fig. 2 Diagrams of the state variable x for all oscillators within the hypernetwork composed of Chen systems at the final time point of simulations ($t = 1000$) for **a** $(\sigma_1, \sigma_2) = (0.36, 0.19)$, **b** $(\sigma_1, \sigma_2) = (0.36, 0.29)$, **c** $(\sigma_1, \sigma_2) = (0.36, 0.41)$, and **d** $(\sigma_1, \sigma_2) = (0.36, 0.81)$. The horizontal axis represents the indices of the nodes (oscillators) in the hypernetwork. The green, red, and blue colors assigned to the nodes correspond to the oscillators belonging to the first, second, and third strong equitable clusters of the hypernetwork, respectively. These diagrams illustrate the sequential emergence of synchronization clusters within the hypernetwork for a fixed coupling strength σ_1 and gradually increasing coupling strength σ_2

hypernetwork composed of Chen systems, as described in Table 1, under varying the coupling strengths σ_1 and σ_2 between the oscillators. In these diagrams, each point represents the average of the synchronization error between the oscillators of the corresponding cluster for the respective coupling strength pair (σ_1, σ_2), according to the color bar. As observed, within the same (σ_1, σ_2) parameter space, clusters predicted at the early stages of the clustering sequence exhibit a wider coherence region than those predicted at later stages.

Figure 4 presents the results of the stability analysis of the predicted synchronization clusters in the hypernetwork based on the MSF approach. Each point of these diagrams represents the maximum of the LLEs corresponding to the respective synchronization cluster, calculated using Eq. 15 and the eigenvalue pairs provided in Table 1, for the associated coupling strength pair (σ_1, σ_2). A comparison between Figs. 3 and 4 reveal a strong agreement between the numerical and analytical findings of the present study.

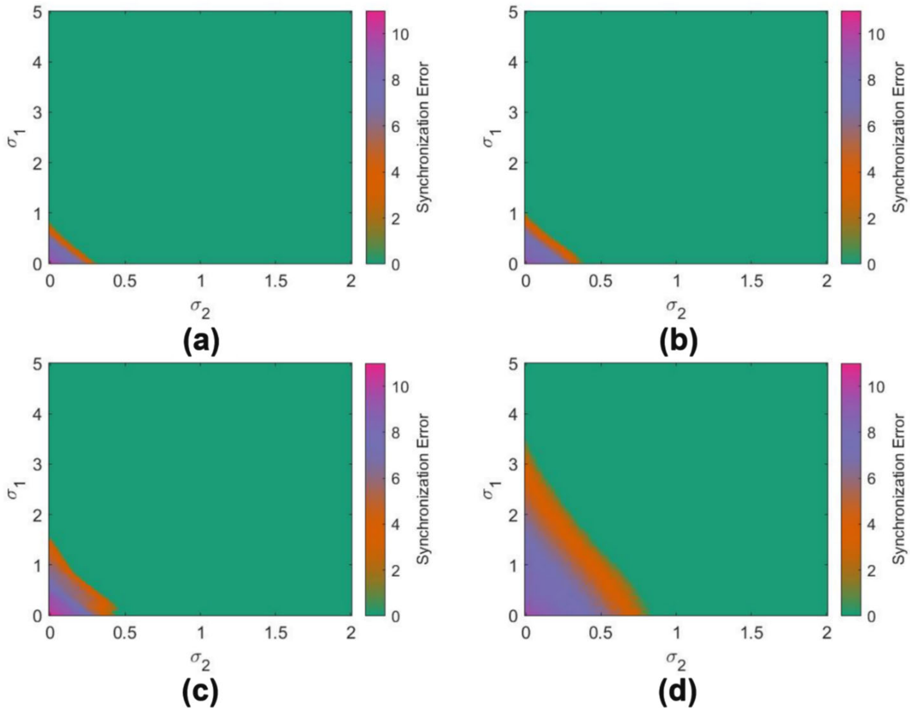

Fig. 3 Diagrams of the average synchronization error for predicted clusters as the coupling strengths σ_1 and σ_2 vary in the hypernetwork composed of Chen systems. Panels correspond to synchronization clusters comprising **a** oscillators 7–10, **b** oscillators 4–6, **c** oscillators 4–10, and **d** oscillators 1–3 of the hypernetwork. In these diagrams, the horizontal axis represents the coupling strength σ_2, and the vertical axis shows the coupling strength σ_1 between the hypernetwork oscillators. The color of each point in these diagrams indicates, according to the colorbar, the average synchronization error among the related cluster oscillators for the corresponding (σ_1, σ_2) pair. These diagrams show that synchronization clusters predicted at later stages of the clustering sequence require higher coupling strengths to emerge within the hypernetwork

3.2 Synchronization Clusters Analysis in the Hypernetwork Composed of Lorenz Systems

This subsection analyses the synchronization clusters and their stability in a hypernetwork composed of Lorenz systems. The dynamics of the hypernetwork nodes are described by the function $F(X) = (\varepsilon(y-x), x(\rho - z) - y, xy - \beta z)^T$ corresponding to the Lorenz system, where $X \equiv (x, y, z)^T$. The parameters of the Lorenz system are chosen as $\varepsilon = 10$, $\rho = 28$, and $\beta = 2$ to ensure chaotic behavior [46].

To construct commutative Laplacian matrices for the different interaction layers of the hypernetwork, the Laplacian matrix $L^2 = L^B$ is first defined based on the Laplacian matrix L^B of graph B shown in Fig. 1, consisting of $N = 10$ nodes, representing the second interaction layer. Subsequently, following the functional mapping method, the Laplacian matrix for the first interaction layer is constructed as $L^1 = \sqrt[3]{L^B} + 0.6L^B$. The coupling

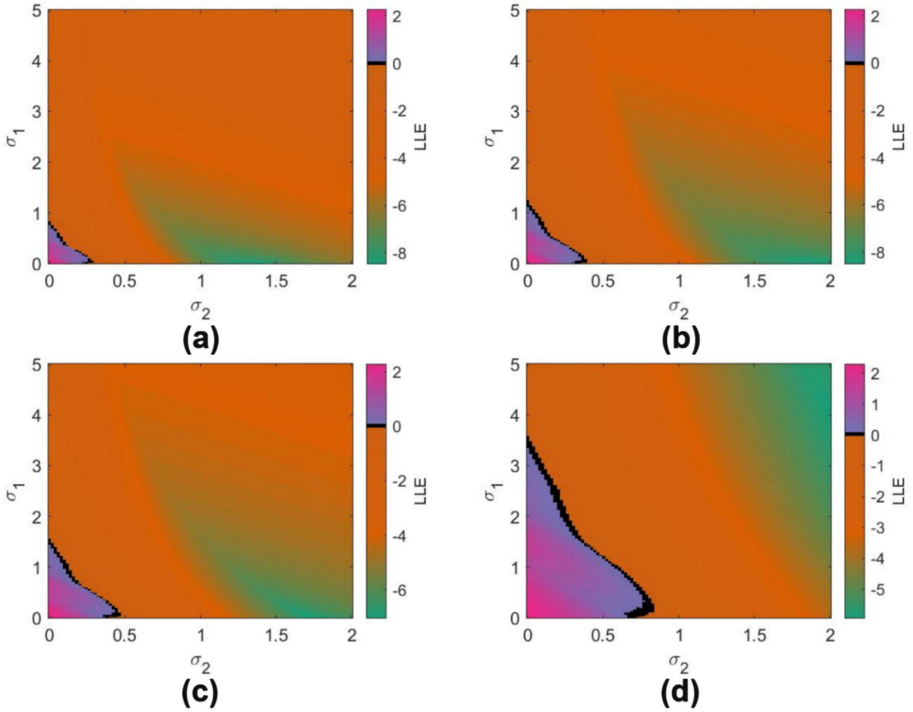

Fig. 4 Diagrams of the maximum LLE for predicted synchronization clusters as the coupling strengths σ_1 and σ_2 vary in the hypernetwork composed of Chen systems. Panels correspond to synchronization clusters comprising **a** oscillators 7–10, **b** oscillators 4–6, **c** oscillators 4–10, and **d** oscillators 1–3 of the hypernetwork. In these diagrams, the horizontal axis represents the coupling strength σ_2, and the vertical axis shows the coupling strength σ_1 between the hypernetwork oscillators. Each point of these diagrams indicates, according to the colorbar, the maximum value of the LLEs calculated based on Eq. 15 for the related cluster and the corresponding (σ_1, σ_2) pair. Comparing these diagrams with those of Fig. 3 shows a good agreement between the numerical and analytical findings of the present study

between oscillators within the first and second interaction layers is implemented as linear-diffusive coupling functions according to the following coupling matrices,

$$g^1 = \begin{bmatrix} 1 & 0 & 0 \\ 0 & 0 & 0 \\ 0 & 0 & 0 \end{bmatrix}, g^2 = \begin{bmatrix} 0 & 0 & 0 \\ 1 & 0 & 0 \\ 0 & 0 & 0 \end{bmatrix}.$$

Both Laplacian matrices, L^1 and L^2, are simultaneously diagonalizable using an orthogonal matrix Q based on Eq. 7. The sequence of synchronization clusters formation in this hypernetwork is predicted by applying the method proposed in Sect. 2.3 to this orthogonal matrix Q, as reported in Table 1. It is noteworthy that, since the Laplacian of one of the interaction layers in both the Chen- and Lorenz-based hypernetworks commutes with the Laplacian of graph B in Fig. 1, a similar clustering structure is observed in both hypernetworks despite their distinct Laplacians. Consequently, the predicted sequence of synchronization cluster formation in both hypernetworks, as stated in the first and second columns of Table 1, is identical. However, the eigenvectors orthogonal to the synchronization manifolds of clusters and their corresponding eigenvalue pairs (the third and fourth columns of Table 1) differ for the same clusters between the two hypernetworks. This results in distinct coupling strength pairs (σ_1, σ_2) required for the emergence of equivalent synchronization clusters in the two hypernetworks.

In the following, Fig. 5 shows the average synchronization error for various clusters in the hypernetwork composed of Lorenz oscillators as the coupling strength pairs (σ_1, σ_2) vary in the interval of [0, 2.5]. Comparison of the synchronized and desynchronized regions in these diagrams indicates that clusters predicted at the later stages of the clustering sequence require higher coupling strengths σ_1 and σ_2 to emerge in the hypernetwork compared to clusters predicted at the earlier stages of the sequence. Accordingly, the synchronized region in the same parameter space (σ_1, σ_2) is wider for clusters predicted at the beginning of the clustering sequence than for those predicted at the end.

Following the stability analysis of the predicted synchronization clusters according to Sect. 2.4, Fig. 6 presents the maximum of the LLEs calculated for these clusters in the hypernetwork of Lorenz oscillators based on Eq. 15 by varying the coupling strength pairs (σ_1, σ_2). Comparison of the results in Figs. 5 and 6 demonstrates excellent agreement between the numerical and analytical findings obtained in this study.

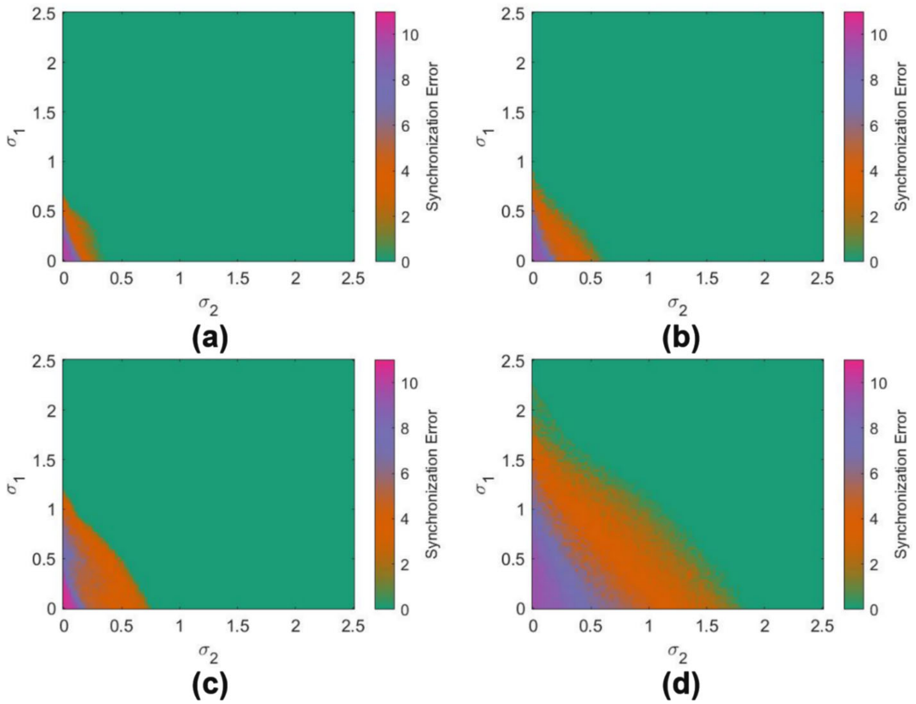

Fig. 5 Diagrams of the average synchronization error for predicted clusters as the coupling strengths σ_1 and σ_2 vary in the hypernetwork composed of Lorenz systems. Panels correspond to synchronization clusters comprising **a** oscillators 7–10, **b** oscillators 4–6, **c** oscillators 4–10, and **d** oscillators 1–3 of the hypernetwork. In these diagrams, the horizontal axis represents the coupling strength σ_2, and the vertical axis shows the coupling strength σ_1 between the hypernetwork oscillators. The color of each point in these diagrams indicates, according to the colorbar, the average synchronization error among the related cluster oscillators for the corresponding (σ_1, σ_2) pair. These diagrams show that synchronization clusters predicted at later stages of the clustering sequence require higher coupling strengths to emerge within the hypernetwork

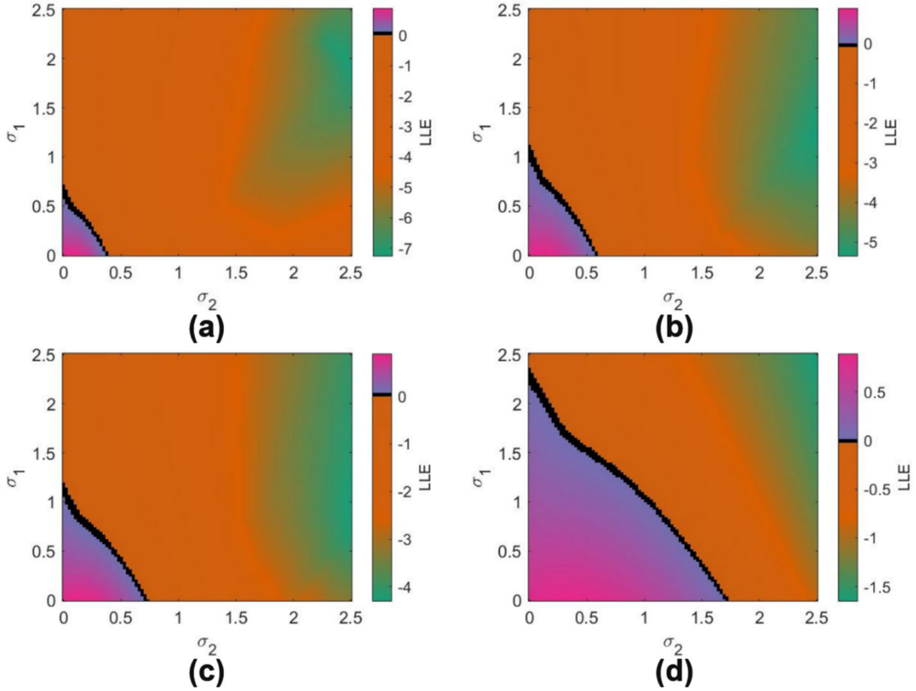

Fig. 6 Diagrams of the maximum LLE for predicted synchronization clusters as the coupling strengths σ_1 and σ_2 vary in the hypernetwork composed of Lorenz systems. Panels correspond to synchronization clusters comprising **a** oscillators 7–10, **b** oscillators 4–6, **c** oscillators 4–10, and **d** oscillators 1–3 of the hypernetwork. In these diagrams, the horizontal axis represents the coupling strength σ_2, and the vertical axis shows the coupling strength σ_1 between the hypernetwork oscillators. Each point of these diagrams indicates, according to the color bar, the maximum value of the LLEs calculated based on Eq. 15 for the related cluster and the corresponding (σ_1, σ_2) pair. Comparing these diagrams with those of Fig. 5 shows a good agreement between the numerical and analytical findings of the present study

4 Discussion and Conclusion

The present study introduced a spectral-based analytical framework for predicting synchronization clusters and assessing their stability in networks comprising multiple commuting interaction layers. While earlier works have focused primarily on complete synchronization [32, 35–37] or on symmetry-based approaches that require explicit identification of group-theoretic structures [30, 41], the framework proposed here provided a mathematically rigorous yet computationally efficient alternative. By exploiting the commutativity of Laplacian matrices across different interaction layers, the method established a unified eigenspace that enabled both the prediction of the full sequence of synchronization cluster formation and the stability analysis through a decoupled Master Stability Function (MSF). This formulation bridges the gap between single-layer spectral methods and the complexity of multilayer architectures, offering a coherent foundation for understanding how diverse interaction mechanisms collectively shape cluster synchronization patterns in hypernetworks.

The analytical and numerical findings demonstrated that, under commuting Laplacians, the entire sequence of synchronization cluster formation can be predicted directly from the shared eigenvectors and eigenvalues of the interaction layers. The predicted clusters exhibited a hierarchical emergence, with smaller, tightly synchronized groups forming at lower coupling strengths and progressively merging into larger coherent structures as coupling increased. This process culminated in complete synchronization, in full agreement with theoretical predictions derived from the shared Laplacian eigenspace. The close correspondence between analytically predicted and numerically observed cluster formations in both Chen- and Lorenz-based hypernetworks confirmed the robustness and generality of the proposed framework. The results further revealed that eigenvalue pairs associated with eigenvectors orthogonal to a cluster's synchronization manifold play a decisive role in determining local stability. Clusters emerging early in the sequence corresponded to eigenmodes with larger eigenvalues, requiring weaker coupling for stabilization and exhibiting broader stability regions in the coupling-parameter space. Conversely, clusters forming later in the hierarchy required stronger coupling strengths to stabilize, resulting in narrower stable regions. These relationships quantitatively linked spectral properties to the dynamical stability landscape of multilayer networks.

A key conceptual insight from this work concerns the role of commutativity among interaction layers. When the Laplacian matrices of different layers are pairwise commuting, the coexistence of multiple coupling mechanisms does not lead to destructive interference among their eigenmodes. Instead, the system preserves a set of orthogonal collective modes that can be analyzed independently. This property greatly simplifies the stability problem, yielding an exact analytical decomposition of multilayer synchronization dynamics. From a broader perspective, this finding suggests that structural compatibility between interaction layers—manifested as spectral commutativity—serves as an organizational principle promoting coherent, clustered behavior in complex systems. Although the commutativity of Laplacian matrices is a strong structural assumption, it holds in some relevant classes of multilayer and hypernetwork systems. Exact commutativity arises when interaction layers share an identical clustering architecture, layers generated from a common eigenbasis, or layers related through functional mappings of a reference Laplacian. Such structures are encountered in some engineered systems (e.g., multilayer power grids with aligned control layers), brain and biological networks exhibiting conserved modular organization across interaction modes, and multiplex networks designed with correlated or hierarchically constrained connectivity patterns. Commuting Laplacians can also emerge as accurate approximations in empirical systems where interlayer correlations are strong, even if exact commutativity is not strictly satisfied. When the commutativity condition is weakly violated, the Laplacians no longer admit an exactly shared eigenbasis, leading to weak coupling between transverse modes that are decoupled under exact commutativity. In this case, the proposed framework remains informative to leading order, as the dominant clustering structure and associated synchronization sequence are primarily governed by the nearly common eigenspaces.

The proposed framework also extends the reach of spectral approaches by demonstrating that mathematical tools developed for single-layer systems can be generalized to hypernetworks without explicit symmetry detection. From a computational perspective, the proposed framework offers a significant advantage over symmetry-based group-theoretic approaches. The dominant computational cost of the present method is associated with the simultaneous diagonalization of the M commuting Laplacian matrices, which for undirected networks can be achieved using standard eigendecomposition algorithms with polynomial complexity in the network size N. Importantly, this procedure is performed once and yields a common eigenbasis, which is subsequently used to predict the entire clustering sequence and to perform stability analysis across all layers. The additional cost scales linearly with the number of layers M, since each layer contributes only an eigenvalue spectrum in the shared basis.

In contrast, group-theoretic methods for cluster synchronization require explicit identification of network automorphisms and symmetry groups for each interaction layer, followed by the construction of quotient networks and block-diagonalization of the dynamics. The computational complexity of symmetry detection grows rapidly with network size and can become combinatorially expensive for large-scale or multilayer systems. Therefore, by avoiding explicit symmetry enumeration and relying solely on the spectral properties of commuting Laplacians, the proposed framework provides a scalable, computationally efficient alternative for analyzing synchronization clusters in hypernetworks with multiple interaction layers.

Comparative analyses using Chen and Lorenz oscillators further underscored the universality of the framework. Despite differences in intrinsic oscillator dynamics and coupling functions, both hypernetworks exhibited identical sequences of cluster formation dictated solely by the shared Laplacian eigenspace. This finding confirms that the spectral structure of the hypernetwork—not the specific oscillator model or coupling function—governs the qualitative pattern of cluster emergence. Nonetheless, the precise coupling strengths required for stabilization varied between systems, reflecting the influence of oscillator dynamics and coupling functions on quantitative stability boundaries. This duality highlights that while topology and spectral organization determine the qualitative structure of synchronization clusters, the quantitative stability characteristics depend on local dynamical details.

Although the numerical results presented in this study focused on relatively small hypernetworks with a limited number of interaction layers, the proposed framework is not restricted to these specific settings. The prediction of synchronization clusters and their stability relies fundamentally on the existence of strong equitable partitions and the commutativity of the Laplacian matrices, rather than on the absolute network size or particular cluster sizes. As a result, the same spectral procedure can be applied directly to larger networks, where the number of nodes N and the sizes of the clusters may vary significantly. In such cases, the common eigenbasis of the commuting Laplacians continues to encode the hierarchical clustering structure, while the decoupled MSF formulation remains valid for assessing cluster stability. Moreover, the framework can be extended to hypernetworks with an arbitrary number of interaction layers, since each additional layer adds an extra spectral component to the eigenvalue tuples governing stability without altering the underlying clustering architecture. Different cluster sizes change the dimensionality of the transverse subspaces associated with each cluster, but do not modify the conceptual steps of the analysis. Therefore, the examples provided in the present study should be viewed as representative illustrations of a general spectral mechanism for predicting and analyzing synchronization clusters in commuting multilayer networks, rather than as special or limiting cases.

Also, the proposed framework was developed under the assumptions of identical oscillator dynamics and exact structural conditions, including strong equitable partitions. However, these conditions may be only approximately satisfied due to parameter mismatch, external noise, or small structural perturbations. In such cases, exact cluster synchronization is generally replaced by approximate cluster synchronization, where nodes within the same predicted cluster remain close but not identical in state space. Small mismatches in oscillator parameters or weak noise sources typically lead to bounded fluctuations around the synchronization manifold and may slightly shift the stability boundaries predicted by the MSF, without fundamentally altering the hierarchical sequence of cluster formation determined by the spectral structure. Similarly, slight deviations from strong equitable partitions introduce heterogeneity in the external inputs received by nodes within the same cluster, which can weaken cluster invariance but does not immediately destroy the clustering pattern when perturbations are small. In this case, the shared eigenspaces of the nearly commuting Laplacians continue to capture the dominant collective modes, and the predicted clustering sequence remains a useful approximation.

From a methodological standpoint, the exact dynamical and structural assumptions adopted in the present study, together with slight deviations from them, provide conceptual clarity and analytical tractability. At the same time, they naturally suggest several important directions for future research. In particular, many real-world systems exhibit interaction layers that are only partially commuting or weakly correlated. Strong violations of commutativity may induce mode mixing and compromise the fully decoupled MSF analysis developed here. Extending the framework to such settings, for instance, through perturbative treatments around a commuting reference structure or approximate joint diagonalization techniques, could elucidate how near-commuting multilayer architectures influence multiscale coordination and cluster stability. Another important extension concerns the assumption of static network topologies. In many biological, technological, and social systems, coupling structures evolve in response to internal dynamics or external stimuli. Incorporating time-varying or adaptive multilayer interactions would further enhance the applicability of the framework and enable the study of dynamically evolving clustering patterns, cluster transitions, and hierarchical desynchronization in realistic systems.

Beyond these open theoretical directions, the proposed spectral framework offers several promising practical implications. It provides a scalable analytical tool for predicting and analyzing cluster synchronization in systems with multiple coupling mechanisms, and introduces a unifying spectral perspective that may guide the design of multilayer networks with prescribed cluster-based functionality. In particular, by engineering commuting Laplacians with targeted eigenvalue distributions, one could control the order, robustness, and stability of cluster formation, enabling selective promotion, suppression, or reconfiguration of synchronization patterns. Finally, the explicit link between observed clustering dynamics and the shared eigenspaces of multilayer Laplacians suggests potential applications in network inference. Transitions between synchronization clusters may serve as indirect signatures of underlying multilayer connectivity, offering a route to reconstruct or constrain structural information from dynamical data alone. Together, these perspectives position the present framework as a foundation for exploring control, inference, and information segregation in multilayer systems, while also motivating future extensions beyond the idealized assumptions considered here.

In summary, this study proposed and validated a spectral-based analytical framework capable of predicting and characterizing synchronization clusters in networks with multiple commuting interaction layers. Theoretical predictions derived from the shared Laplacian eigenspace showed excellent agreement with numerical simulations across distinct oscillator dynamics and coupling functions, confirming the robustness of the approach. By integrating spectral graph theory with the MSF formalism, the framework provided a conceptually elegant and computationally efficient route to understanding the hierarchical organization and stability of cluster synchronization in hypernetworks. Future extensions to non-commuting or adaptive hypernetworks, as well as applications to neural, communication, or power-grid systems, may further reveal how spectral compatibility governs coordination in complex multilayer systems.

Appendix: Stability Analysis of Complete Synchronization in Single-Interaction Networks

The MSF framework offers a powerful analytical tool for evaluating the local stability of complete synchronization in networks comprising identical oscillators [38]. Consider a network of N oscillators coupled through a diffusive coupling function $G : R^n \to R^n$, each governed by the n-dimensional state vector $X_i(t) \in R^n$. The temporal evolution of the i th oscillator can be written based on the Laplacian matrix L of the network as follows.

$$\dot{X}_i = F(X_i) - \sigma \sum_{j=1}^{N} L_{ij} G\big(X_j\big) \quad i = 1, 2, \ldots, N, \tag{17}$$

where $F : R^n \to R^n$ describes the intrinsic node dynamics, σ is the coupling strength between oscillators, and L is the Laplacian matrix with dimension $N \times N$ describing the network topology. Under the diffusive coupling function, the completely synchronized state is defined by $X_1 = X_2 = \cdots = X_N = X_s$, where $X_s(t)$ evolves according to the isolated oscillator dynamics $\dot{X}_s = F(X_s)$. To examine the local stability of this synchronous manifold, small perturbations $\delta X_i = X_i - X_s$ are introduced. Linearizing the network equations around the synchronized trajectory yields the following equation.

$$\delta\dot{X}_i = DF(X_s)\delta X_i - \sigma \sum_{j=1}^{N} L_{ij} DG(X_s)\delta X_j \quad i = 1, 2, \ldots, N. \tag{18}$$

In Eq. 18, $DF(X_s)$ and $DG(X_s)$ denote the Jacobian matrices of F and G, respectively, evaluated at X_s. By stacking all perturbation vectors into a composite state vector $\delta X = [\delta X_1{}^T, \delta X_2{}^T, \ldots, \delta X_N{}^T]^T$, the linearized system can be compactly expressed in Kronecker form as follows.

$$\delta\dot{X} = (I_N \otimes DF(X_s) - \sigma L \otimes DG(X_s))\delta X. \tag{19}$$

Since the Laplacian L is real and symmetric, it can be diagonalized as $L = P\Lambda P^T$, where P is the matrix of orthonormal eigenvectors and $\Lambda = diag(\mu_1, \mu_2, \ldots, \mu_N)$ contains the Laplacian eigenvalues ordered as $0 = \mu_1 < \mu_2 \le \cdots \le \mu_N$. Applying the modal transformation $\eta = \big(P^T \otimes I_n\big)\delta X$, the system decouples into N independent subsystems of dimension n as stated in Eq. 20.

$$\dot{\eta}_i = (DF(X_s) - \sigma\mu_i DG(X_s))\eta_i \quad i = 1, 2, \ldots, N. \tag{20}$$

The first mode ($\mu_1 = 0$) corresponds to perturbations parallel to the synchronization manifold and therefore does not affect its stability. The remaining $N-1$ modes, each governed by $\dot{\eta} = (DF(X_s) - \zeta DG(X_s))\eta$, with $\zeta = \sigma\mu_i$, describe perturbations transverse to the synchronization manifold. The LLE of this system defines the MSF. If LLE is negative for all $\zeta = \sigma\mu_i (i = 2, \ldots, N)$, all transverse perturbations decay exponentially, and the completely synchronized state is locally stable. This formalism elegantly separates the influence of nodal dynamics from the influence of network structure encoded in the Laplacian spectrum. As a result, the MSF framework enables a universal characterization of synchronization stability that is applicable across various network topologies, coupling configurations, and oscillator dynamics.

Author Contributions Conceptualization was carried out by Sheida Ansarinasab and Matjaž Perc. Formal analysis and investigation were performed by Sheida Ansarinasab and Fatemeh Parastesh. Methodology was contributed by Karthikeyan Rajagopal. Supervision was provided by Farnaz Ghassemi and Sajad Jafari. The original draft of the manuscript was written by Sheida Ansarinasab and Fatemeh Parastesh, while writing—review & editing was carried out by Farnaz Ghassemi, Karthikeyan Rajagopal, Sajad Jafari, and Matjaž Perc. All authors read and approved the final manuscript.

Funding M.P. was supported by the Slovenian Research and Innovation Agency (Javna agencija za znanstvenoraziskovalno in inovacijsko dejavnost Republike Slovenije, Grant No. P1-0403).

Data Availability All data and simulation codes used in this study will be made available at reasonable request via the following link: https://drive.google.com/file/d/1cwaS4NTXgIXKgoW9BlOq2B5_GOAsMEOD/view?usp=drive_link.

Declarations

Conflict of interest The authors have no competing interests to declare that are relevant to the content of this article.

References

1. Majeed, A., Rauf, I.: Graph theory: a comprehensive survey about graph theory applications in computer science and social networks. Inventions **5**(1), 10 (2020)
2. Centonze, M.S., Treves, A., Agliari, E., Barra, A.: Analytical methods for continuous attractor neural networks. J. Stat. Phys. **192**(5), 67 (2025). https://doi.org/10.1007/s10955-025-03447-4
3. Agliari, E., Fachechi, A., Duarte Mourão, P.: The beneficial role of noises for disentanglement tasks in modular Hebbian networks. Physica A **682**, 131134 (2026). https://doi.org/10.1016/j.physa.2025.131134
4. Rahimi Saryazdi, A., Ghassemi, F., Tabanfar, Z., Ansarinasab, S., Nazarimehr, F., Jafari, S.: EEG-based deception detection using weighted dual perspective visibility graph analysis. Cogn. Neurodyn. **18**(6), 3929–3949 (2024). https://doi.org/10.1007/s11571-024-10163-4
5. Klinshov, V.V., Kovalchuk, A.V., Soloviev, I.A., Maslennikov, O.V., Franović, I., Perc, M.: Extending dynamic memory of spiking neuron networks. Chaos Solitons Fractals **182**, 114850 (2024). https://doi.org/10.1016/j.chaos.2024.114850
6. Klinshov, V.V., Kovalchuk, A.V., Franović, I., Perc, M., Svetec, M.: Rate chaos and memory lifetime in spiking neural networks. Chaos Solitons Fractals **158**, 112011 (2022). https://doi.org/10.1016/j.chaos.2022.112011
7. Zhou, Y., Luo, X., Zhou, M.: Cryptocurrency transaction network embedding from static and dynamic perspectives: an overview. IEEE/CAA J. Autom. Sin. **10**(5), 1105–1121 (2023). https://doi.org/10.1109/JAS.2023.123450
8. Yue, Y., Li, X., Zhang, D., Wang, S.: How cryptocurrency affects economy? A network analysis using bibliometric methods. Int. Rev. Financ. Anal. **77**, 101869 (2021). https://doi.org/10.1016/j.irfa.2021.101869
9. Moradi, M., Panahi, S., Zhai, Z.-M., Weng, Y., Dirkman, J., Lai, Y.-C.: Heterogeneous reinforcement learning for defending power grids against attacks. APL Mach. Learn. (2024). https://doi.org/10.1063/5.0216874
10. Amani, A.M., Jalili, M.: Power grids as complex networks: resilience and reliability analysis. IEEE Access **9**, 119010–119031 (2021). https://doi.org/10.1109/ACCESS.2021.3107492
11. Samoylenko, I., Aleja, D., Primo, E., Alfaro-Bittner, K., Vasilyeva, E., Kovalenko, K., et al.: Why are there six degrees of separation in a social network? Phys. Rev. X **13**(2), 021032 (2023). https://doi.org/10.1103/PhysRevX.13.021032
12. Özer, M., Perc, M.: Impact of social networks on the labor market inequalities and school-to-work transitions. Yükseköğretim Derg. **11**(1), 38–50 (2021). https://doi.org/10.2399/yod.21.868353
13. Nazerian, A., Panahi, S., Sorrentino, F.: Synchronization in networks of coupled oscillators with mismatches. Europhys. Lett. **143**(1), 11001 (2023). https://doi.org/10.1209/0295-5075/acde5f
14. Nazerian, A., Panahi, S., Sorrentino, F.: Synchronization in networked systems with large parameter heterogeneity. Commun. Phys. **6**(1), 253 (2023). https://doi.org/10.1038/s42005-023-01355-1
15. Ansarinasab, S., Parastesh, F., Ghassemi, F., Rajagopal, K., Jafari, S., Kurths, J.: Optimized multi-variable coupling can improve synchronization in complex networks. Nonlinear Dyn. **112**(20), 18491–18500 (2024). https://doi.org/10.1007/s11071-024-09934-9

16. Zhou, P., Ma, J., Xu, Y.: Phase synchronization between neurons under nonlinear coupling via hybrid synapse. Chaos Solitons Fractals **169**, 113238 (2023). https://doi.org/10.1016/j.chaos.2023.113238
17. Majhi, S., Ghosh, S., Pal, P.K., Pal, S., Pal, T.K., Ghosh, D., et al.: Patterns of neuronal synchrony in higher-order networks. Phys. Life Rev. **52**, 144–170 (2025). https://doi.org/10.1016/j.plrev.2024.12.013
18. Khan, M.S., Petroni, A., Biagi, M.: Cooperative communication based protocols for underwater wireless sensors networks: a review. Sensors **24**(13), 4248 (2024)
19. Fu, Y., Mechitov, K., Hoang, T., Kim, J.R., Memon, S.A., Spencer, B.F., Jr.: Efficient and high-precision time synchronization for wireless monitoring of civil infrastructure subjected to sudden events. Struct. Control. Health Monit. **28**(1), e2643 (2021). https://doi.org/10.1002/stc.2643
20. Rai, I., C, S.: Microgrid and grid synchronization: a critical analysis of challenges and opportunities. Electr. Power Syst. Res. **242**, 111434 (2025). https://doi.org/10.1016/j.epsr.2025.111434
21. Prymushko, A., Puchko, I., Yaroshynskyi, M., Sinko, D., Kravtsov, H., Artemchuk, V.: Efficient state synchronization in distributed electrical grid systems using conflict-free replicated data types. IoT **6**(1), 6 (2025)
22. Tang, J., Zhang, J., Ma, J., Luo, J.: Noise and delay sustained chimera state in small world neuronal network. Sci. China Technol. Sci. **62**(7), 1134–1140 (2019). https://doi.org/10.1007/s11431-017-9282-x
23. Schöll, E.: Partial synchronization patterns in brain networks. Europhys. Lett. **136**(1), 18001 (2021). https://doi.org/10.1209/0295-5075/ac3b97
24. Ansarinasab, S., Bayani, A., Parastesh, F., Ghassemi, F., Rajagopal, K., Jafari, S.: Transition to synchronization in functional brain networks of children suffering from ADHD. Brain Struct. Funct. **230**(5), 82 (2025). https://doi.org/10.1007/s00429-025-02935-3
25. Franović, I., Eydam, S., Semenova, N., Zakharova, A.: Unbalanced clustering and solitary states in coupled excitable systems. Chaos Interdiscip. J. Nonlinear Sci. (2022). https://doi.org/10.1063/5.0077022
26. Shahriari, Z., Parastesh, F., Jalili, M., Berec, V., Ma, J., Jafari, S.: The role of coupling factors on the emergence of synchronization and chimera patterns in network of non-locally coupled pancreatic β-cells. Europhys. Lett. **125**(6), 60001 (2019). https://doi.org/10.1209/0295-5075/125/60001
27. Bayani, A., Nazarimehr, F., Jafari, S., Kovalenko, K., Contreras-Aso, G., Alfaro-Bittner, K., et al.: The transition to synchronization of networked systems. Nat. Commun. **15**(1), 4955 (2024). https://doi.org/10.1038/s41467-024-48203-6
28. Wang, J., Liu, X.: Cluster synchronization for multi-weighted and directed complex networks via pinning control. IEEE Trans. Circuits Syst. II **69**(3), 1347–1351 (2022). https://doi.org/10.1109/TCSII.2021.3108116
29. Timofeyev, T., Patania, A.: Cluster Synchronization via Graph Laplacian Eigenvectors. arXiv preprint (2025). arXiv:250318978
30. Zhang, L., Su, L., Li, S., Han, Y., Pan, W., Yan, L., et al.: Regulation of cluster synchronization in multilayer networks of delay coupled semiconductor lasers with the use of disjoint layer symmetry. Opt. Express **32**(2), 1123–1134 (2024). https://doi.org/10.1364/OE.502251
31. Tomaselli, C., Gambuzza, L.V., Sun, G.-Q., Boccaletti, S., Frasca, M.: Taming cluster synchronization. Chaos Solitons Fractals **199**, 116576 (2025). https://doi.org/10.1016/j.chaos.2025.116576
32. Rakshit, S., Bera, B.K., Ghosh, D., Sinha, S.: Emergence of synchronization and regularity in firing patterns in time-varying neural hypernetworks. Phys. Rev. E **97**(5), 052304 (2018). https://doi.org/10.1103/PhysRevE.97.052304
33. Pereda, A.E.: Electrical synapses and their functional interactions with chemical synapses. Nat. Rev. Neurosci. **15**(4), 250–263 (2014). https://doi.org/10.1038/nrn3708
34. Heydari, S., Iñiguez, G., Kertész, J., Saramäki, J.: Disentangling degree and tie strength heterogeneity in egocentric social networks. EPJ Data Sci. **13**(1), 76 (2024). https://doi.org/10.1140/epjds/s13688-024-00513-x
35. Sorrentino, F.: Synchronization of hypernetworks of coupled dynamical systems. N. J. Phys. **14**(3), 033035 (2012). https://doi.org/10.1088/1367-2630/14/3/033035
36. Rakshit, S., Bera, B.K., Bollt, E.M., Ghosh, D.: Intralayer synchronization in evolving multiplex hypernetworks: analytical approach. SIAM J. Appl. Dyn. Syst. **19**(2), 918–963 (2020). https://doi.org/10.1137/18m1224441
37. Ansarinasab, S., Ghassemi, F., Parastesh, F.: The combined impact of structure and coupling type on synchronization dynamics in hypernetworks. Chaos Solitons Fractals **199**, 116892 (2025). https://doi.org/10.1016/j.chaos.2025.116892
38. Pecora, L.M., Carroll, T.L.: Master stability functions for synchronized coupled systems. Phys. Rev. Lett. **80**(10), 2109–2112 (1998). https://doi.org/10.1103/PhysRevLett.80.2109
39. Mondal, A., Khanra, P., Ghosh, S., Kundu, P., Hens, C., Pal, P.: Enhancing cluster synchronization in phase-lagged multilayer networks. Chaos Solitons Fractals **200**, 117053 (2025). https://doi.org/10.1016/j.chaos.2025.117053

40. Ma, C., Yang, Q., Wu, X., Lu, J.: Cluster synchronization: from single-layer to multi-layer networks. Chaos Interdiscip. J. Nonlinear Sci. (2019). https://doi.org/10.1063/1.5122699
41. Della Rossa, F., Pecora, L., Blaha, K., Shirin, A., Klickstein, I., Sorrentino, F.: Symmetries and cluster synchronization in multilayer networks. Nat. Commun. **11**(1), 3179 (2020). https://doi.org/10.1038/s41467-020-16343-0
42. Jiang, R., Li, D.: Simultaneous diagonalization of matrices and its applications in quadratically constrained quadratic programming. SIAM J. Optim. **26**(3), 1649–1668 (2016). https://doi.org/10.1137/15m1023920
43. Sagnol, G.: On the semidefinite representation of real functions applied to symmetric matrices. Linear Algebra Appl. **439**(10), 2829–2843 (2013). https://doi.org/10.1016/j.laa.2013.08.021
44. Kovalenko, K., Contreras-Aso, G., del Genio, C.I., Boccaletti, S., Sánchez-García, R.J.: Equitability and explosive synchronisation in multiplex and higher-order networks. arXiv preprint (2025). arXiv:250709319
45. Tan, D., Chen, Z.: On a general formula of fourth order Runge-Kutta method. J. Math. Sci. Math. Educ. **7**(2), 1–10 (2012)
46. Huang, L., Chen, Q., Lai, Y.-C., Pecora, L.M.: Generic behavior of master-stability functions in coupled nonlinear dynamical systems. Phys. Rev. E **80**(3), 036204 (2009). https://doi.org/10.1103/PhysRevE.80.036204

Authors and Affiliations

Sheida Ansarinasab[1] · Farnaz Ghassemi[1] · Fatemeh Parastesh[2,3] · Karthikeyan Rajagopal[2,4] · Sajad Jafari[1,5] · Matjaž Perc[6,7,8,9]

✉ Matjaž Perc
Matjaz.Perc@gmail.com

1 Department of Biomedical Engineering, Amirkabir University of Technology (Tehran Polytechnic), Tehran, Iran

2 Center for Research, Easwari Engineering College, Chennai, India

3 Center for Cognitive Science, Trichy SRM Medical College Hospital and Research Center, Tiruchirappalli, India

4 Center for Research, SRM TRP Engineering College, Tiruchirappalli, India

5 Health Technology Research Institute, Amirkabir University of Technology (Tehran Polytechnic), Tehran, Iran

6 Faculty of Natural Sciences and Mathematics, University of Maribor, Koroška cesta 160, 2000 Maribor, Slovenia

7 Community Healthcare Center Dr. Adolf Drolc Maribor, Ulica talcev 9, 2000 Maribor, Slovenia

8 Department of Physics, Kyung Hee University, 26 Kyungheedae-ro, Dongdaemun-gu, Seoul 02447, Republic of Korea

9 University College, Korea University, 145 Anam-ro, Seongbuk-gu, Seoul 02841, Republic of Korea